Master's Thesis

Performance Assessment of Monolayer Black Arsenic Metal-Oxide-Semiconductor Field Effect Transistors through Valley-Resolved *Ab-Initio* Quantum Transport Simulation

Jae Eun Seo

Department of Electrical Engineering

Ulsan National Institute of Science and Technology

2021

Performance Assessment of Monolayer Black Arsenic Metal-Oxide-Semiconductor Field Effect Transistors through Valley-Resolved *Ab-Initio* Quantum Transport Simulation

Jae Eun Seo

Department of Electrical Engineering

Ulsan National Institute of Science and Technology

Performance Assessment of Monolayer Black Arsenic Metal-Oxide-Semiconductor Field Effect Transistors through Valley-Resolved *Ab-Initio* Quantum Transport Simulation

A thesis/dissertation submitted to
Ulsan National Institute of Science and Technology
in partial fulfillment of the
requirements for the degree of
Master of Science

Jae Eun Seo

06.18.2021 of submission

Approved by

Advisor

Kyung Rok Kim

Performance Assessment of Monolayer Black Arsenic Metal-Oxide-Semiconductor Field Effect Transistors through Valley-Resolved *Ab-Initio* Quantum Transport Simulation

Jae Eun Seo

This certifies that the thesis/dissertation of Jae Eun Seo is approved.

06.18.2021 of submission

Signature

Advisor: Kyung Rok Kim

Signature

Jiwon Chang : Thesis Committee member #1

Signature

Jongwon Lee : Thesis Committee member #2

Abstract

Recently, black arsenic, a mono-elemental two-dimensional (2-D) material, a cousin of black phosphorus, has been proven to have better atmospheric stability and higher mobility than black phosphorus. Here, we present detailed theoretical assessment on device performances of n- and p-metal-oxide-semiconductor field effect transistors (n- and p- MOSFETs) based on monolayer black arsenic. Our study starts with the exploration of basic electronic properties of monolayer black arsenic through *ab-initio* density functional theory (DFT) calculations, and then current transport in the device is investigated using our *in-house* quantum transport simulator which reads in the result of *ab-initio* electronic property simulations. Monolayer black arsenic has a band structure similar to monolayer black phosphorus in that it has a very anisotropic Γ valley. However, it differs from black phosphorus in that it has additional Δ valleys near the Γ valley. By simulating the valley that is the origin of the current, we investigate the role of Γ and Δ valleys for carrier transport in monolayer black arsenics MOSFETs. It also compares and analyzes the effect of crystal orientation and channel length scaling with monolayer black phosphorus MOSFETs. Our simulation results reveal that Δ valleys in monolayer black arsenic lessen the directional dependency of current transport and make monolayer black arsenic more vulnerable to short channel effects (SCEs) due to the increased tunneling current in the extremely scaled device.

Contents

List of Figures

Figure 8. VB edge profiles along with the corresponding energy and current density transmitted from each valley for the 10 nm gate length monolayer black arsenic p-MOSFETs at the off-state in the (a) armchair and (b) zigzag directions and at the on-state in the (c) armchair and (d) zigzag directions.

Figure 9. VB edge profiles along with the corresponding energy resolved current densities for the 10 nm gate length monolayer black phosphorus p-MOSFETs at the off-state in the (a) armchair and (b) zigzag directions and at the on-state in the (c) armchair and (d) zigzag directions.

Figure 10. Transfer characteristics of the 7 nm gate length monolayer black arsenic and monolayer black phosphorus (a) n- and (b) p-MOSFETs at V_{DS} = 0.5 V and -0.5 V, respectively, in the armchair and zigzag directions. *SS* around I_{OFF} is listed.

Figure 11. CB edge profiles and current density transmitted from each valley for the 7 nm gate length monolayer black arsenic n-MOSFETs at the off-state in the (a) armchair and (b) zigzag directions. VB edge profiles along with the corresponding energy and current density from each valley for the 7 nm gate length monolayer black arsenic p-MOSFETs at the off-state in the (c) armchair and (d) zigzag directions.

List of Tables

Nomenclature

MOSFETs	Metal-oxide-semiconductor field effect transistors
SCEs	Short channel effects
2-D	Two-dimensional
DFT	Density functional theory
TB	Tight-binding
CB	Conduction band
VB	Valence band
LDA	Local density approximation
BZ	Brillouin zone
DG	Double-gate
MLWFs	Maximally localized Wannier functions
WFs	Wannier functions
CBM	Conduction band minimum
VBM	Valence band maximum
ITRS	International technology roadmap for semiconductor
SS	Subthreshold slope
TE	Thermionic emission
TN	Tunneling
DOS	Density of states

1. Introduction

After successfully demonstrating the metal-oxide-semiconductor field effect transistors (MOSFETs) with channel material as black phosphorus, black phosphorus was considered to be the two-dimensional (2-D) material with a good prospect to be applied to next-generation device technology because of the decent carrier mobility [1-3], unique transport properties [4, 5] and adjustable band gap [6], However, black phosphorus has a problem of stability when exposed to the surrounding air, and thus, its practical application to real life is still difficult [7]. In recent years, following black phosphorus, arsenic (As), antimony (Sb), and other 2-D materials consisted of only one element are attracting attention as 2-D materials that rise beyond black phosphorus. Mono-elemental 2-D materials belonging to group 15 have a variety of allotropic morphologies [8, 9]. Using density functional theory (DFT) calculation, gray arsenic/antimony is proved to be the most stable in terms of the energy among the various allotropes [9-11]. Also, Electrical properties such as carrier mobility and great immunity to device scaling in monolayer gray arsenic/antimony MOSFETs are explored theoretically by preceding research [9-15]. However, MOSFETs based on channel materials as gray arsenic/antimony has not yet been implemented experimentally. Meanwhile, black arsenic, another arsenic allotrope that forms a puckered honeycomb structure like black phosphorus, is mechanically exfoliated successfully from natural bulk [16, 17]. Black arsenic MOSFETs using channel materials as monolayer and multilayer black arsenic flakes show adequate mobilities, good on/off ratios, highly anisotropic characteristics in carrier and heat transport and good atmospheric stability compared to black phosphorus [16, 17]. Although not yet experimentally confirmed, the theoretically calculated electron mobility and hole mobility of monolayer black arsenic are higher and similar, respectively, when compared to that of monolayer black phosphorus [10]. Until now, several theoretical studies focusing on the material properties of black arsenic have been conducted [10, 17-20], but detailed theoretical studies on the carrier transport of devices based on black arsenic have not been conducted.

We show an extensive analysis of carrier transport in the device which has a channel material as a monolayer black arsenic and monolayer black phosphorus. The device performance was evaluated through ballistic carrier transport calculation using an *in-house* simulator in which the DFT-based simulation and the device simulation using the tight-binding (TB) method were combined. and Valley-resolved current analysis is performed to investigate the roles of several valleys near the bandgap in monolayer black arsenic n- and p- MOSFETs, respectively. In addition, the degree of influence of crystal orientation and device scaling on carrier transport was analyzed by comparing with monolayer black phosphorus n- and p- MOSFETs.

2. Methods

2.1 DFT simulation. DFT simulations by OPENMX [21] are performed to study the electronic band structures of monolayer black arsenic using the linear combination of pseudoatomic orbital method with local density approximation (LDA) for the exchange-correlation potentials [22]. A k-point mesh and a mesh cut-off energy are 9×11×1 and 150 Ry for the Brillouin Zone (BZ) integration. Geometry optimization is performed until the maximum residual force becomes smaller than 0.01 Hartree/Bohr.

2.2 Device Simulation. To simulate a device using black arsenic, a double-gate (DG) MOSFET with two gates covering the channel was used. Figure 1(a) show the schematic diagram of simulated device. The device consists with the source/drain electrodes which are semi-infinite and channel of monolayer black arsenic [20]. Channel is undoped but electrodes for source/drain are doped as n-type and p-type with a doping level of 3×10^{13} cm^{-2}, respectively. In the case of simulated devices, HfO_2 with $\kappa = 25$ was used as the gate oxide, and the junction of the source/drain electrode and the channel was aligned with the edge of HfO_2. The gate oxide thickness was fixed at about 3nm for all the devices that were simulated, and the simulation was carried out with 0.5 V V_{DS} applied. Simulations were conducted for devices with 7nm and 10nm channel lengths, and the boundary conditions were set in the direction of the device width.

2.3 Ballistic Transport Simulation. To simulate the ballistic carrier transport of the device, we first use OPENMX [21] to obtain the TB basis set through maximally localized Wannier functions (MLWFs) calculations. In OPENMX, a set of orthogonal MLWFs at the atomic center were obtained from the Bloch wave function by the DFT calculations. Ballistic transport simulator based on the recusive scattering matrix approach load the TB Hamiltonian, which is constituted with Hopping potentials between different Wannier functions (WFs) [23]. Transport equation and Poisson equation are self-consistently combined to solve iteratively together. When the charge density and electrostatic potential coincide with each other, the current is calculated by multiplying the transfer probability and the Fermi function weight.

2.4 Valley-Resolved Current Density Calculation. For transport calculations, as in Figure 2(a), a unit cell (transport unit cell) (dashed light blue) larger than a primitive unit cell (dashed grey) is prepared to accurately reproduced DFT band structures. Connecting transport unit cells in series composes the device. In semi-infinite source/drain, a generalized eigenvalue problem constructed from the onsite Hamiltonian H_{NN} and the coupling Hamiltonian H_{NN+1} defined for the transport unit cells in Figure 2(a) is solved to get the right/left propagating modes. For example, Figure 2(b) shows band structures of monolayer black arsenic for the transport unit cell in source at transverse mode $k_y = 0$. Since the transport unit cell is 2 times larger in x- and y- directions, respectively, than the primitive unit cell, band structures are folded as compared to those from the primitive unit cell in Figure 1(b). In Figure 2(a),

there are 6 propagating modes (3 left (filled circles) and 3 right (empty circles) propagating modes) at the energy level 0 eV where the source fermi level is located. We can find out the direction of propagating modes by calculating current from each mode. Current per mode per energy between any two transport unit cells N and N+1 can be obtained from

$$j = \frac{2\pi e}{h}\mathrm{Im}(C^*\psi_N^* H_{NN+1} C\psi_{N+1})$$

where ψ is the wave function, h is the Plank's constant, and C is a normalization constant for current per mode per energy to be equal to $\frac{e}{h}$. Modes with positive current ($j > 0$) are right propagating and are injected into channel. Current calculation for each mode can also be helpful to identify the propagating modes belonging to the specific valley since it tells group velocity of the mode. We use group velocities and wave vectors of the right propagating modes to figure out valley where each mode resides in. For example, At the energy level 0.1 eV in Figure 2(b), group velocities of right propagating modes are higher for Δ valleys (green empty circles) than for Γ valley (blue empty circle). At the energy level 0 eV, two right propagating modes from Δ valleys (green empty circles) have larger absolute values of wave vectors than that from Γ valley (blue empty circle). Following these procedures, current can be selectively calculated for each valley.

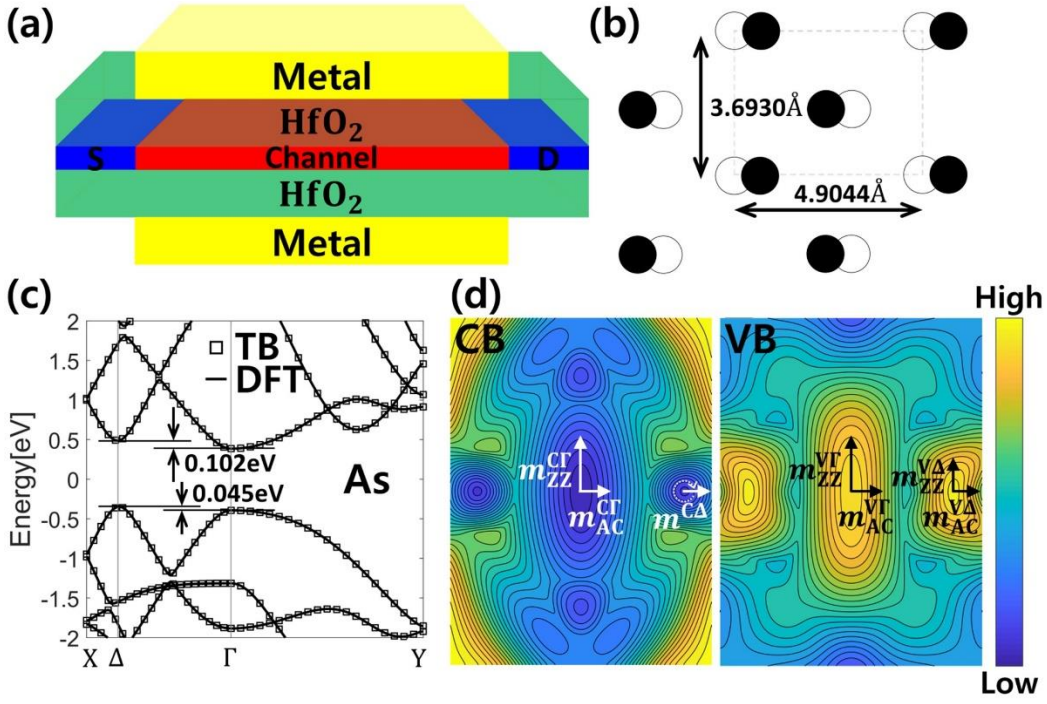

Figure 1. (a) Device configuration of DG monolayer black arsenic MOSFETs with the HfO_2 gate oxide thickness T_{OX} = 3 nm and the channel length $L_G \approx$ 10 nm. (b) Top view of monolayer black arsenic (c) Band structures of monolayer black arsenic calculated from TB and DFT. (d) Energy contour plots of the CBM and the VBM for monolayer black arsenic.

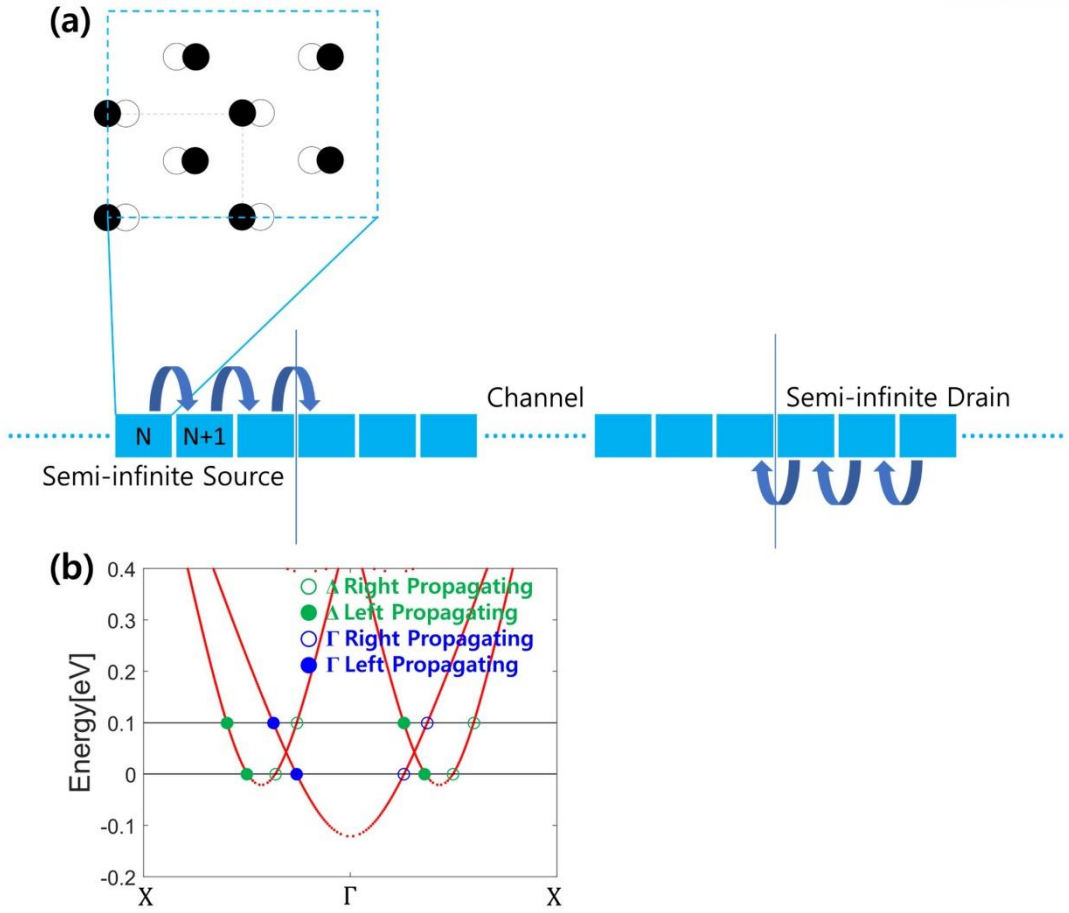

Figure 2. (a) A unit cell (transport unit cell) used in transport calculations of monolayer black arsenic MOSFETs directed in the armchair direction and schematic representation of modes propagation in the device. (b) Band structures of monolayer black arsenic calculated from TB for the transport unit cell in source at transverse mode $k_y = 0$.

3. Results and Discussion

3.1 Electronic properties of black Arsenic and black Phosphorus. Crystal structure of monolayer black arsenic is shown in Figure 1(b). As Similar as monolayer black phosphorus, 4 arsenic atoms, which are arranged in a puckered honeycomb structure, make up a rectangular primitive unit cell. For armchair and zigzag directions, the lattice constants of primitive unit sell are a_{AC}= 4.904 Å and a_{ZZ}= 3.693 Å, respectively. These values are calculated by geometry optimization in DFT calculation and they are similar values with the preceding studies [17-20]. In figure 1(c), we show the band structures along high symmetric points (X–Γ–Y) in the 1st BZ calculated by TB (square) method and DFT (line) calculation. 3 Wfs are formed for each arsenic atom, and in the case of monolayer black arsenic, a total of 12 WFs are generated because there are total of 4 arsenic atoms in a primitive unit cell. Therefore, in the transport calculations, we consider a total of 12 bands around the band gap. As shown in Figure 1(c), it can be confirmed that the band structures calculated by TB and DFT are almost identical. From the band structure, it can be seen that conduction band minimum (CBM) is located at point Γ and valence band maximum (VBM) is at Δ point in the direction from the Γ point to X point, thus having an indirect band gap E_{Gap} = 0.734 eV. It is also well known that DFT using LDA underestimates a band gap. In our MOSFETs simulation, however, CBs and VBs are separately considered for n- and p-MOSFETs, respectively. Therefore, device performances predicted by our quantum transport simulations are not affected by the band gap value. From Figure 1(c), we observe other CB and VB valleys near CBM and VBM, respectively, in energy. The second lowest CB valley (Δ point : ~ 0.102eV higher than CBM) and the second highest VB valley (Γ point : ~ 0.045 eV lower than VBM) are located close enough to CBM and VBM, respectively. Thus, these valleys in close proximity to CBM and VBM may affect carrier injection. As seen in the energy contour plot of the lowest CB and the highest VB of monolayer black arsenic in Figure 1(d), Γ valleys show highly anisotropic whereas two-fold degenerate Δ valleys are almost isotropic or less anisotropic compared with Γ valley. We extract effective masses for 2 carriers (electron and hole) of Γ and Δ valleys by the parabolic fitting of band structures in the armchair (Γ→X) and zigzag (Γ→Y) directions, respectively, as listed in Table 1. For Γ valleys, the armchair direction has light effective masses $m_{AC}^{C\Gamma}$= 0.239×m_e for CB and $m_{AC}^{V\Gamma}$= 0.205×m_e for VB, but in the zigzag direction, CB has $m_{ZZ}^{C\Gamma}$= 1.269×m_e and VB has $m_{ZZ}^{V\Gamma}$= 2.009×m_e which are ~5 and ~ 10 times heavier. Otherwise, in the effective masses of Δ valleys, unlike the Γ valleys, there is a large difference between CB and VB. Isotropic Δ valleys in CB has a light effective mass $m^{C\Delta}$= 0.101×m_e, but anisotropic Δ valleys in VB has a light effective mass $m_{AC}^{V\Delta}$= 0.102×m_e in armchair direction and a relatively heavy effective mass $m_{ZZ}^{V\Delta}$ = 0.449×m_e in the zigzag direction. For monolayer black phosphorus, anisotropic valleys at Γ point has light effective mass in the armchair direction and heavy effective mass in the zigzag direction as similar as black arsenic. The effective masses for black

phosphorus according to the direction are summarized in Table 2. The band structures and energy contour plots are shown in Figure 3(a) and (b) for monolayer black phosphorus. What distinguishes monolayer black arsenic from monolayer black phosphorus is the two-fold degenerate Δ valleys. Since Δ and Γ valleys are very close in energy, both valleys may possibly supply sizable current in monolayer black arsenic MOSFETs while current is dominated by Γ valleys in monolayer black phosphorus MOSFETs.

Transport Direction	**Effective Mass for black Arsenic**			
	Electron		**Hole**	
	Δ	**Γ**	**Δ**	**Γ**
Armchair (Γ→X)	0.101	0.239	0.102	0.205
Zigzag (Γ→Y)	0.101	1.269	0.449	2.009

Table 1. Electron and hole effective masses of monolayer black arsenic in Γ and Δ valleys in the armchair (Γ→X) and zigzag (Γ→Y) directions

Transport Direction	**Effective Mass for black Phosphorus**	
	Electron	**Hole**
	Γ	**Γ**
Armchair (Γ→X)	0.121	0.121
Zigzag (Γ→Y)	1.174	1.651

Table 2. Electron and hole effective masses of monolayer black phosphorus in Γ valley in the armchair (Γ→X) and zigzag (Γ→Y) directions

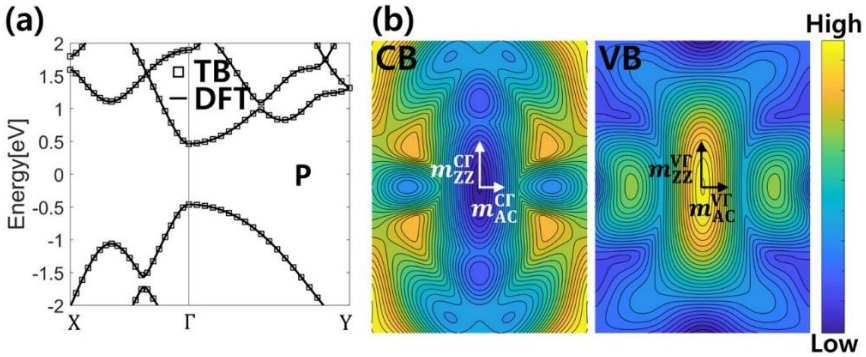

Figure 3. (a) Band structures of monolayer black phosphorus. (b) Energy contour plots of the CBM and the VBM for monolayer black phosphorus.

3.2 Transfer Characteristics for 10nm channel n-MOSFETs. In Figure 4, with V_{DS} = 0.5 V applied, transfer characteristics (I_{DS}-V_{GS}) of the 10 nm gate length monolayer black arsenic (red) n-MOSFETs aligned in the armchair (circle) and zigzag (triangle) directions, respectively are presented and compared with those of single-layer black phosphorus (grey) n-MOSFETs. We adjust V_{GS} such that the off-state (V_{DS} = V_{DD} = 0.5 V and V_{GS} = 0 V) current I_{OFF} is 0.1 μA/μm according to the ITRS requirements for high performance devices [24]. From the log scale plot, decent subthreshold slope (*SS*) estimated around I_{OFF} is observed in both monolayer black arsenic and monolayer black phosphorus n-MOSFETs, regardless of transport directions. The zigzag direction results in slightly better *SS* than the armchair direction for both channel materials, indicating a little dependency of subthreshold characteristics on the transport direction. As seen in Figure 4, the transport directional dependency becomes substantial as V_{GS} increases. At the on-state (V_{DS} = V_{GS} = V_{DD} = 0.5 V), monolayer black arsenic n-MOSFETs offers I_{ON} ≈ 4075 μA/μm in the armchair direction and 2175 μA/μm in the zigzag direction. The current becomes maximum when flowing in the direction of armchair because of the heavy transverse effective mass and light longitudinal effective mass of Γ valley, the valley of conduction band minimum. Similar on-state current (I_{ON}) characteristics can be confirmed in monolayer black phosphorus n-MOSFETs. It is larger in the armchair direction (I_{ON} ≈ 4582 μA/μm) than in the zigzag direction (I_{ON} ≈ 1775 μA/μm). Dependency on the direction of transport is stronger in the device based on monolayer black phosphorus since the anisotropic Γ valley is the main valley that injects carriers into the channel in monolayer black phosphorus, while, in monolayer black arsenic, the degenerate Δ valleys positioned ~ 0.102 eV above Γ valley in CB, also contribute nonnegligible amount of current. Therefore, the range of I_{ON} that can be obtained is wider in monolayer black phosphorus (1775 ~ 4582 μA/μm) than in monolayer black arsenic (2175 ~ 4075 μA/μm).

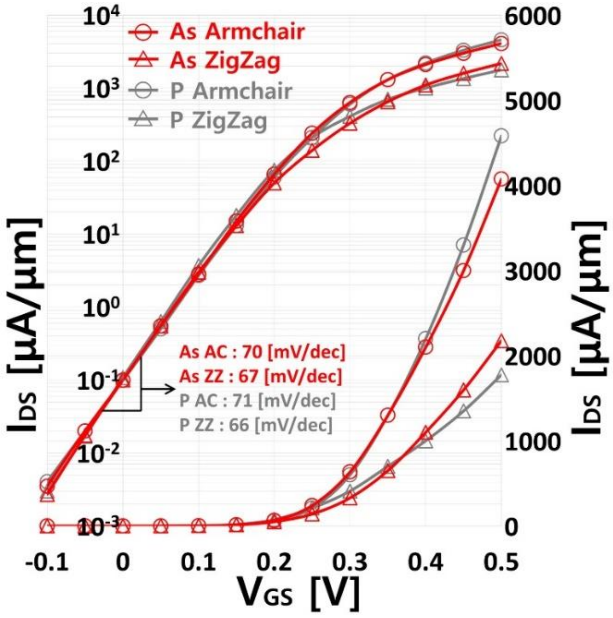

Figure 4. Transfer characteristics of the 10 nm gate length monolayer black arsenic and monolayer black phosphorus n-MOSFETs in the armchair and zigzag directions at V_{DS} = 0.5 V. *SS* around I_{OFF} is listed.

3.3 Current components for 10nm channel n-MOSFETs. To understand the carrier transport in more detail, CB edge profiles (red dashed line) and current densities along the corresponding energy at the on- and off-states for the armchair and zigzag directions, respectively, are presented in Figure 5. In the plots which is for 10nm gate length monolayer black arsenic n-MOSFETs, source and drain Fermi levels are denoted by E_{FS} and E_{FD}, respectively, and E_{FS} is set on an energy reference.

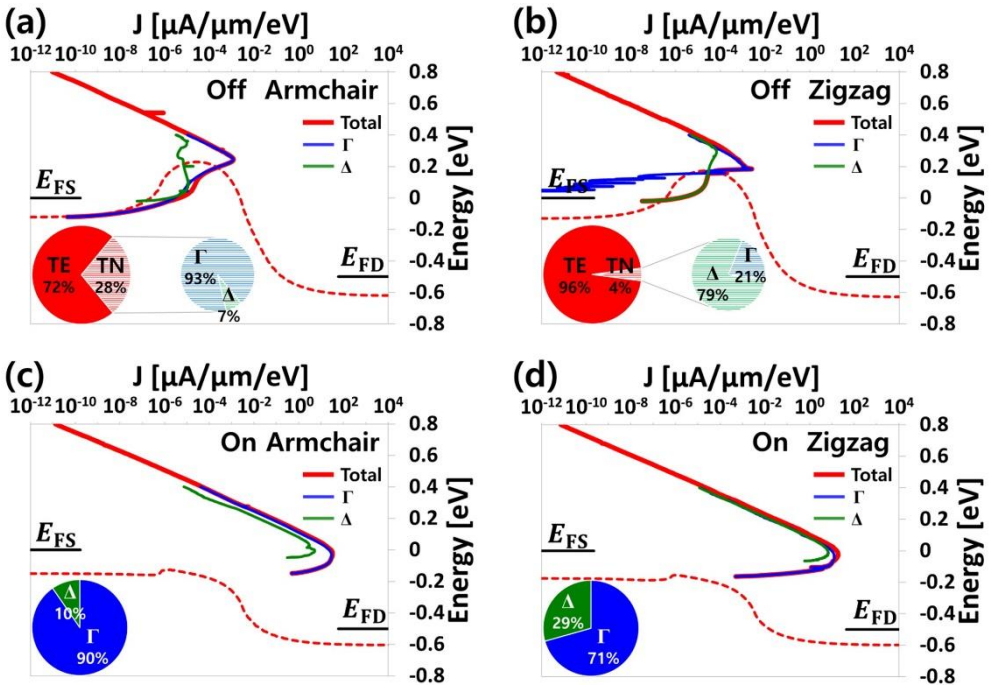

Figure 5. CB edge profiles along with the corresponding energy and current density transmitted from each valley for the 10 nm gate length monolayer black arsenic n-MOSFETs at the off-state in the (a) armchair and (b) zigzag directions and at the on-state in the (c) armchair and (d) zigzag directions.

At the off-state in Figure 5(a) and (b), I_{OFF} consists of the source-drain direct tunneling (TN) current as well as the thermionic emission (TE) current in the device based on monolayer black arsenic for both transport directions. As shown in pie chart, we calculate the ratios of the TE (solid red) and TN (striped red) currents to I_{OFF}, respectively, indicating that ~ 28 % and ~ 4 % of I_{OFF} are the TN currents in the armchair and zigzag directions, respectively. Tunneling current reduction in the zigzag direction explains slightly better *SS* mentioned above. The off-state is analyzed further through valley-resolved current densities. In the armchair direction, significant tunneling is expected for both Δ and Γ valleys because of the light transport effective masses ($m^{C\Delta}$= 0.101×m_e and $m_{AC}^{C\Gamma}$= 0.239×m_e), which is confirmed by quite large current densities below the potential barrier from both valleys in Figure 5(a) and (b). As seen in the pie chart presenting the valley composition of the TN current in I_{OFF}, Γ valley (striped blue) dominantly supplies (~ 93 %) the TN current while Δ valley (striped green) contributes only ~ 7 %. The reason is that Γ valley is more populated since it is positioned ~ 0.102 eV closer to the Fermi level and capable of providing large density of states (DOS) owing to the heavy transverse

effective mass ($m_{ZZ}^{C\Gamma}$= 1.269×m_e). In the zigzag direction (Figure 5(b)), on the other hand, the Γ valley current density (blue) below the potential barrier becomes negligible because of the heavy transport effective mass. But, substantial current from Δ valley (green) still passes through the barrier because Δ valley is isotropic with a light effective mass. Hence, as opposed to the armchair direction, most of the TN current (~ 79 %) comes from Δ valley. However, as tunneling from Γ valley providing most of the TN current in the armchair direction is well suppressed in the zigzag direction, the amount of the TN current is much less (~ 4 % of I_{OFF}), suggesting more efficient managing of the source-to-drain direct tunneling and the consequent slightly better *SS* in the zigzag direction. For the on-state, we calculated the relative ratio of current to I_{ON} from Δ (green) and Γ (blue) valleys and plotted in the pie chart of Figure 5(c) and (d). In both directions, we confirm that the most of I_{ON} comes from Γ valley which is the lowest valley of conduction band. In the armchair direction where the anisotropic Γ valley has light longitudinal effective mass and heavy transverse effective mass, the portion of Γ valley becomes higher (~ 90 %) than that of zigzag direction (~ 71 %). High injection velocity from light transport effective mass and large DOS of Γ valley from heavy transverse effective mass in the armchair direction increase the carrier injection to channel of black arsenic and thus maximize I_{ON} in black arsenic n-MOSFETs. Understanding carrier injection in monolayer black phosphorus n-MOSFETs is relatively clear and easy because there are no other valleys near Γ valley. As seen in Figure 6, once Γ valley is directed towards the armchair direction for the light longitudinal effective mass, the TN current in I_{OFF} is significant due to high injection velocity, and I_{ON} is boosted. But, the zigzag direction yields dramatic reduction of the TN current and I_{ON}. In monolayer black arsenic n-MOSFETs, the highly anisotropic Γ valley is the lowest CB valley, which is the main contributor of the total current. Therefore, despite the two-fold degenerate Δ valleys with an isotropic light effective mass, dependency of I_{ON} on the direction of transport is still evident, but not as much as in monolayer black phosphorus. Meanwhile, at the off-state, even if the TN current is suppressed effectively in the zigzag direction, the TE current is more prominent (~ 72 % and ~ 96 % of I_{OFF} in the armchair and zigzag directions, respectively) in the 10 nm gate length device. So, the subthreshold conduction is properly managed in both transport directions, leading to the negligible directional dependency and decent *SS*.

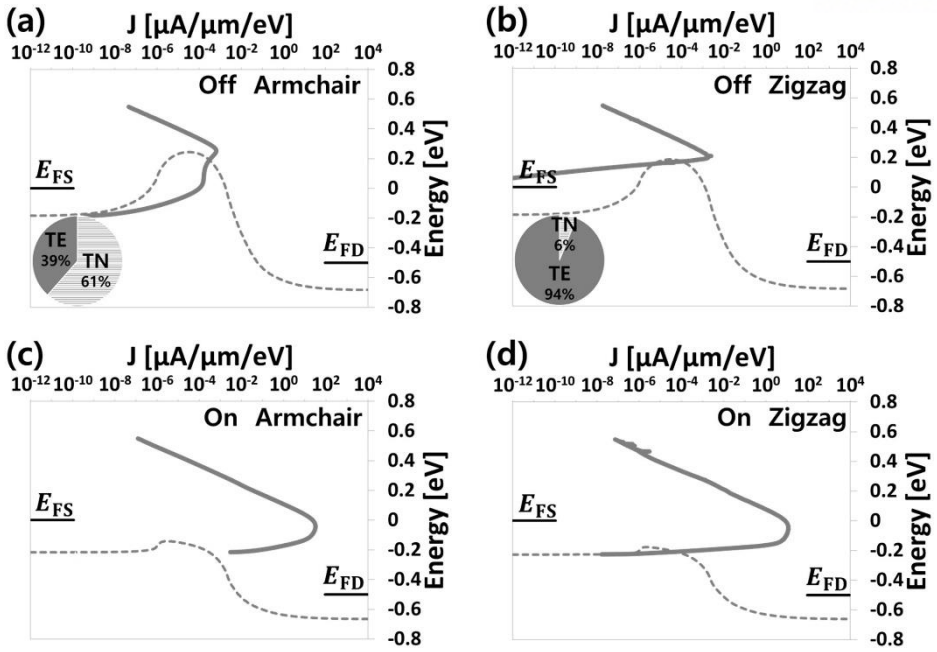

Figure 6. CB edge profiles along with the corresponding energy resolved current densities for the 10 nm gate length monolayer black phosphorus n-MOSFETs at the off-state in the (a) armchair and (b) zigzag directions and at the on-state in the (c) armchair and (d) zigzag directions.

3.4 Transfer Characteristics for 10nm channel p-MOSFETs. Figure 7 compares transfer characteristics of monolayer black arsenic (red) and monolayer black phosphorus (grey) p-MOSFETs in the armchair (circle) and zigzag (triangle) directions, respectively, at V_{DS} = −0.5 V. From the log scale plot, we observe decent subthreshold characteristics for both black arsenic and black phosphorus, irrespective of channel orientation, in the 10 nm gate length scale. As similar as in n-MOSFETs, a little improved *SS* is also achievable in p-MOSFETs directed in the zigzag direction. Meanwhile, the linear scale of transfer characteristics shows the sensitivity of current in the channel orientation for increasing V_{GS}. Monolayer black arsenic p-MOSFETs provides I_{ON} ≈ 4308 μA/μm in the armchair direction and 2000 μA/μm in the zigzag direction. The maximum I_{ON} is from the armchair direction where the carrier injection rate and DOS are the largest. Comparing with the monolayer black arsenic n-MOSFETs, the armchair direction I_{ON} is slightly higher (~ +6 %) while the zigzag direction I_{ON} is reduced (~ −8 %) in p-MOSFETs, indicating an increased dependency of channel orientation. As previously discussed with Figure 1(c) and (d), Γ valley in VB shows a higher degree of anisotropy with a roughly ~ 10 times heavier effective mass in the zigzag direction than in the armchair direction while about ~ 5 times for Γ valley in CB. Moreover, two-fold degenerate Δ valleys are also anisotropic ($m_{AC}^{V\Delta}$= 0.102×m_e and $m_{ZZ}^{V\Delta}$= 0.449×m_e) in VB, but isotropic ($m^{C\Delta}$= 0.101×m_e) in CB. Thus, carrier injection is slightly more sensitive to the alignment of the channel crystal in the p-MOSFETs. As similar as n-MOSFETs, the anisotropy in I_{ON} is more pronounced in monolayer black phosphorus p-MOSFETs than in monolayer black arsenic p-MOSFETs. In monolayer black phosphorus, the second highest CB valleys and the

second lowest VB valleys are a few hundred meV away from CBM and VBM, which maximizes the effect of the highly anisotropic Γ valley on current transport. However, in monolayer black arsenic, isotropic or less anisotropic two-fold degenerate Δ valleys near Γ valley diminishes anisotropy.

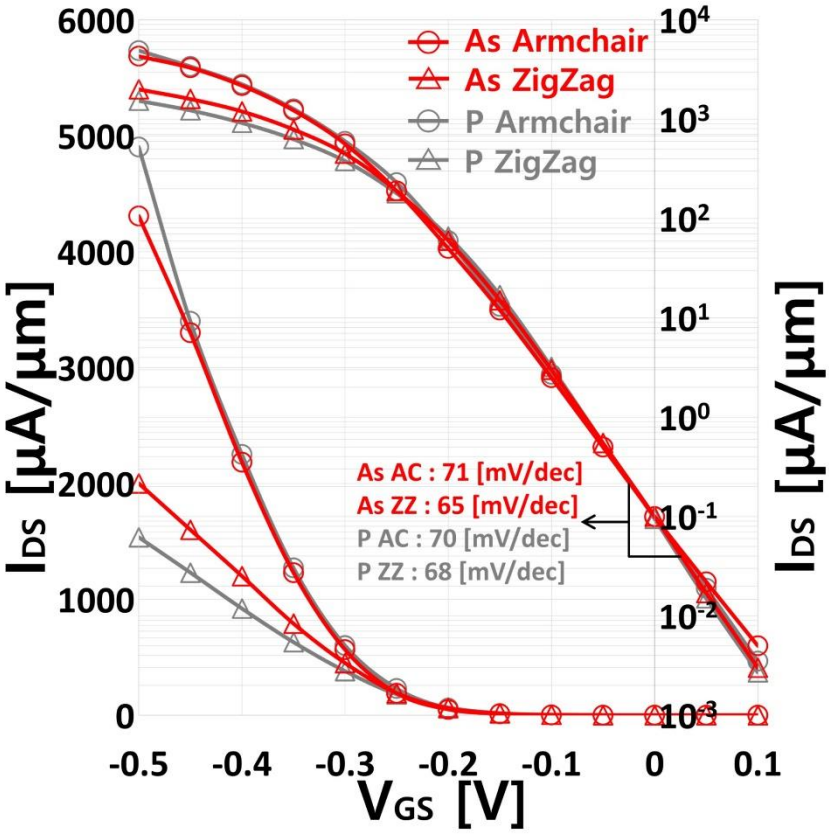

Figure 7. Transfer characteristics of the 10 nm gate length monolayer black arsenic and monolayer black phosphorus p-MOSFETs in the armchair and zigzag directions at V_{DS} = -0.5 V. *SS* around I_{OFF} is listed.

3.5 Current component for 10nm channel p-MOSFETs. In Figure 8, the carrier transport of monolayer black arsenic p-MOSFETs is analyzed by comparing the VB edge profiles (dashed red) for the corresponding energy and the current densities transmitted from 2 kinds of valleys in the on- and off-states. At the off-state, the ratio of TE (solid red) and TN (striped red) currents to I_{OFF} are calculated and in particular, the ratio of the valley where the current compositing the TN current comes out is further investigated in pie charts. For the armchair direction in Figure 8(a), the TN current (striped red) is prominent, comprising ~ 75 % of I_{OFF}, because both Δ and Γ valleys are aligned to have light transport and heavy transverse effective masses, thereby maximizing tunneling current. The high TN current is mostly ascribed to Δ valley (striped green) rather than Γ valley (striped blue) as shown in the pie chart noting ~ 99 % of the TN current from Δ valley. Since two-fold degenerate Δ valleys are the highest in VB and the transport effective mass ($m_{AC}^{V\Delta}$= 0.102×m_e) is about half of that in Γ valley ($m_{AC}^{V\Gamma}$= 0.205×m_e), the TN current is dominated by Δ valley. For such reasons, as compared to n-MOSFETs where Γ valley

is more predominant than Δ valley, the TN current of p-MOSFETs in the armchair direction is greatly enhanced (~ 2.7 times more). As we select the transport direction as the zigzag direction in Figure 8(b), tunneling current density below the barrier is considerably prohibited due to the increase of transport effective masses, and hence the amount of the TN current decreases to ~ 6 %. Most of the TN current (~ 99 %) still originates from Δ valley because of the relatively light effective mass ($m_{ZZ}^{V\Delta}$= 0.449×m_e). At the on-state, from the pie chart in Figure 8(c) and (d), we observe that there is more carrier injection supplied by the Δ valley in both transport directions (~ 66 % in the armchair and ~ 79 % in the zigzag). This is because Δ valley with two-fold degeneracy and anisotropy is the VBM valley. Comparing from which valley the current density comes from in armchair and zigzag directions, the current density from the Γ valley (blue) decrease more than the current density from the Δ valley (green) in the zigzag direction. Although the Δ and Γ valleys of VB are both anisotropic, the effective masses of Δ and Γ valleys in the zigzag direction are ~ 4 and ~ 10 times heavier, respectively. Therefore, the direction of transport has a stronger influence on the Γ valley current. Carrier injection in monolayer black phosphorus p-MOSFETs is very similar to n-MOSFET counterpart. This is because the VB of monolayer black phosphorus also features a highly anisotropic Γ valley. The armchair direction yields the highest TN current in I_{OFF}, but it is effectively suppressed in the zigzag direction as in Figure 9.

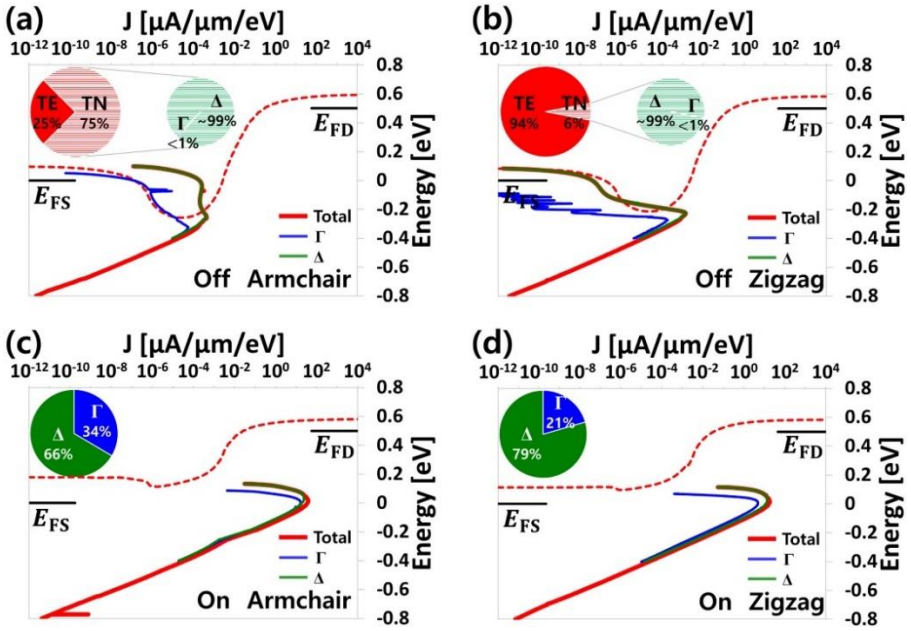

Figure 8. VB edge profiles along with the corresponding energy and current density transmitted from each valley for the 10 nm gate length monolayer black arsenic p-MOSFETs at the off-state in the (a) armchair and (b) zigzag directions and at the on-state in the (c) armchair and (d) zigzag directions.

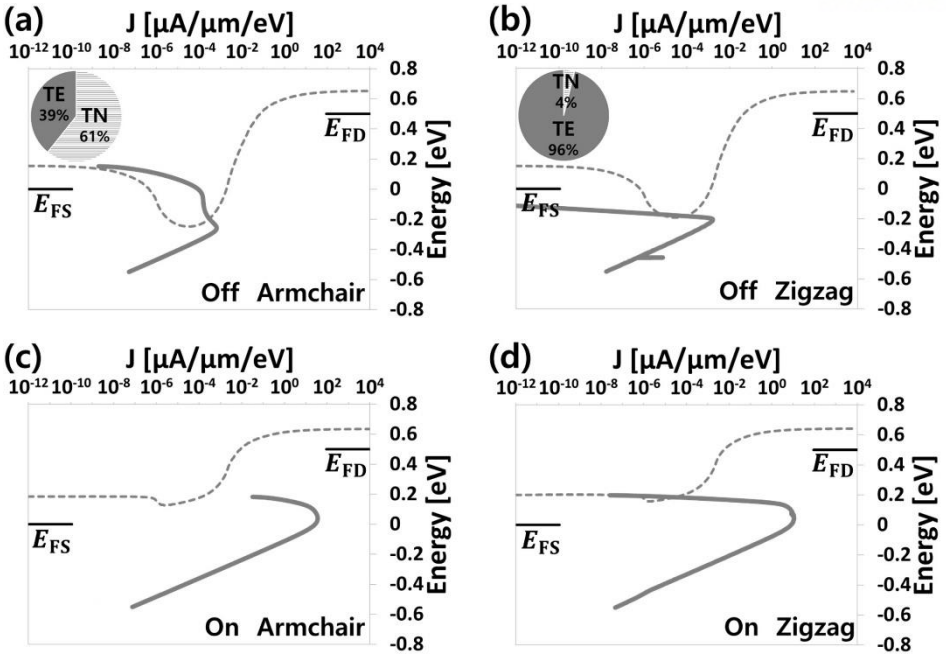

Figure 9. VB edge profiles along with the corresponding energy resolved current densities for the 10 nm gate length monolayer black phosphorus p-MOSFETs at the off-state in the (a) armchair and (b) zigzag directions and at the on-state in the (c) armchair and (d) zigzag directions.

3.6 Effects of Device Scaling. Benchmarking against monolayer black phosphorus MOSFETs, in the 10 nm gate length scale where tunneling through the channel barrier is still in the acceptable level, we observe almost same subthreshold characteristics in both channel materials. However, the dependency of I_{ON} on the transport direction is relatively weak in monolayer black arsenic due to the presence of the Δ valleys. As a result, higher I_{ON} is obtainable in monolayer black phosphorus n- and p-MOSFETs. To examine scaling behavior of monolayer black arsenic MOSFETs, we simulate the 7 nm gate length device while keeping all other device parameters the same. Transfer characteristics of the 7 nm gate length n- and p- MOSFETs are plotted in Figure 10(a) and (b), respectively. As observed in the log scale plot, scaling a gate length deteriorates subthreshold characteristics for all channel materials in both transport directions, but with different degrees of degradation. For n-MOSFETs in Figure 10(a), the *SS* of monolayer black arsenic was degraded to 89 mV/dec and 84 mV/dec in the armchair direction and zigzag direction. On the other hand, the case of monolayer black phosphorus, *SS* deteriorated the most (104 mV/dec) in the armchair, but still showed good *SS* value (69 mV/dec) in the zigzag direction. For p-MOSFETs in Figure 10(b), the explicit dependency of *SS* on the transport direction is confirmed in the case of the device based on black arsenic. *SS* significantly deteriorate in the armchair direction (116 mV/dec) but the degree of degradation in the zigzag direction is minimal (72 mV/dec). For monolayer black phosphorus p-MOSFETs, *SS* is about 95 mV/dec in the armchair direction and about 67 mV/dec in the zigzag direction, respectively. The tendency of *SS* increasement due to scaling of devices based on monolayer black phosphorus can be easily understood because both CB and VB are characterized

only by Γ valleys, which exhibit approximately the same degrees of anisotropy for CB and VB. According to previous papers [25, 26], scaling affects more severely to monolayer black phosphorus in the armchair direction for n- and p-MOSFETs due to enhanced tunneling current below the potential barrier. On the other hands, the scaling effect of monolayer black arsenic MOSFETs is quite different with monolayer black phosphorus MOSFETs due to Δ valleys which are existed near Γ valley.

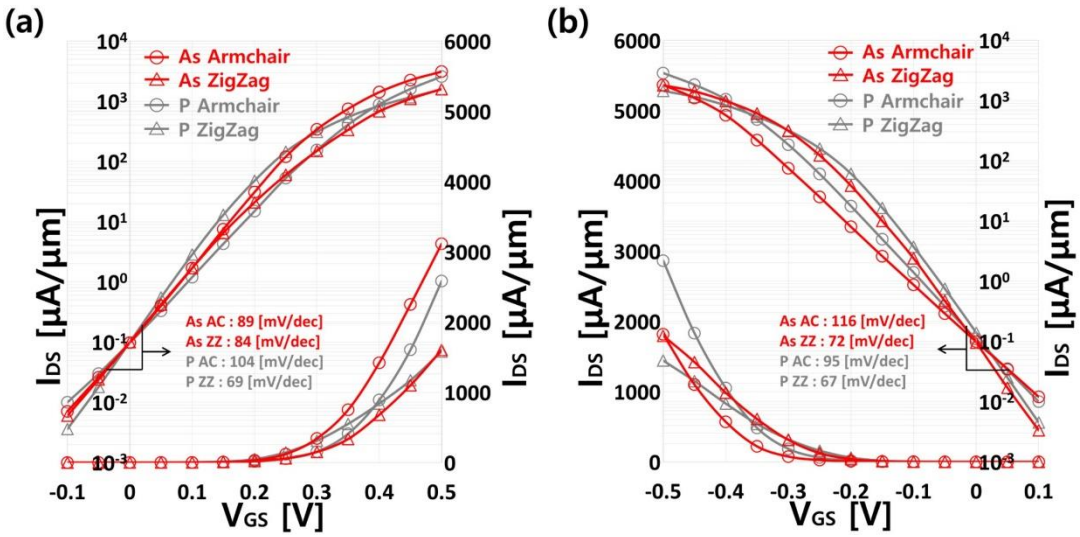

Figure 10. Transfer characteristics of the 7 nm gate length monolayer black arsenic and monolayer black phosphorus (a) n- and (b) p-MOSFETs at V_{DS} = 0.5 V and -0.5 V, respectively, in the armchair and zigzag directions. *SS* around I_{OFF} is listed.

As shown in Figure 11, The role of Δ valley in monolayer black arsenic MOSFETs is explored by plotting the CB and VB edge profiles (dashed red) for the corresponding energy and analyzing which valley the current density originates from at the off-state. Compared to the 10 nm gate length device (Figure 5(a) and (b) for n-MOSFETs and Figure 8(a) and (b) for p-MOSFETs), the direct tunneling from source to drain is enhanced in all cases because the tunneling barrier width is shorten in the scaled short channel device. As can be seen in Figure 11(a) and (b), in the case of n-MOSFETs, the tunneling current density originated from the Γ valley, which is very anisotropic, is dominant only in the armchair direction. This not only makes the ratio of the TN current (~ 73 %) higher but also has a worse *SS* than in the zigzag direction. Therefore, in order to meet the same I_{OFF} target (0.1 μA/μm), a potential barrier should be raised to prevent the TN current in the armchair direction than in the zigzag direction as shown in CB edge profiles in Figure 11(a) and (b). However, since the Δ valley (green), which has a light isotropic effective mass ($m^{C\Delta}$= 0.101×m_e), also creates a lot of carrier injection by tunneling, it weakens the effect of the Γ valley and deteriorates *SS* in the zigzag direction as much as in the armchair direction. For p-MOSFETs in the armchair direction (Figure 11(c)), which shows the worst *SS* ≈ 116 mV/dec, the potential barrier in channel cannot prevent the source carriers from tunneling to drain. Therefore, most of I_{OFF} (~ 99 %) occurs from the TN current (striped red) as seen in the pie chart.

Meanwhile, in the zigzag direction (Figure 11(d)), since both Δ and Γ valleys are aligned in a direction with heavy longitudinal effective mass, the ratio of TN current decreases sharply (~ 24 %). This leads to a result with good *SS* ≈ 72 mV/dec and it is possible to have a relatively lower potential barrier to have the same I_{OFF}. As in the 10 nm gate length device, two-fold degenerate Δ valleys, the highest VB valleys, with the lightest transport mass contribute the most TN current (striped green) in all directions. In the device based on monolayer black arsenic, the TN current from Γ valley has a similar dependence on the direction of transport in both n- and p-MOSFETs, which has high TN current in the armchair direction and low TN current in the zigzag direction. But, in n- and p- MOSFETs, the TN current originating from the Δ valley shows a different trend according to the transport direction. In n-MOSFETs, the tunneling current densities derived from the isotropic Δ valley of CB does not show any difference depending on the transport direction while tunneling current occurring in the anisotropic Δ valley of VB is only conducted significantly in the armchair direction, but it can still be managed in the zigzag direction in p-MOSFETs. Therefore, device scaling deteriorates *SS* equally in all directions in the case of n-MOSFETs, but for p-MOSFETs, it degrades seriously only in the armchair direction and its effect is minimized in the zigzag direction.

With the aggressively scaled gate length below 10 nm, monolayer black phosphorus would also be a better channel material in terms of subthreshold characteristics. Decent *SS* is still possible in monolayer black phosphorene MOSFETs by adjusting the transport direction in the heavy transport mass direction of Γ valley. But, in monolayer black arsenic, Δ valleys which are isotropic or less anisotropic than Γ valley degrade *SS* more in all directions, and thus lead to worse *SS* than in monolayer black phosphorus.

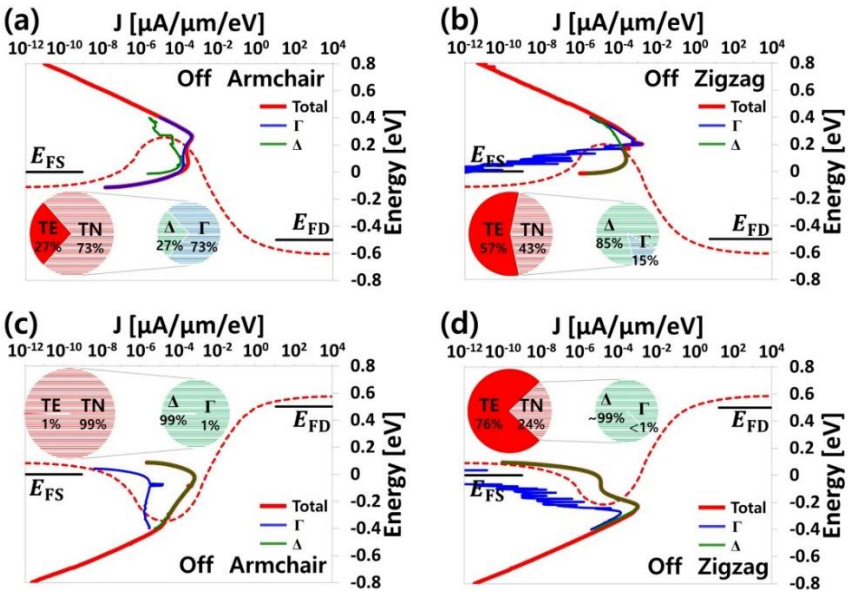

Figure 11. CB edge profiles and current density transmitted from each valley for the 7 nm gate length monolayer black arsenic n-MOSFETs at the off-state in the (a) armchair and (b) zigzag directions. VB edge profiles along with the corresponding energy and current density transmitted from each valley for the 7 nm gate length monolayer black arsenic p-MOSFETs at the off-state in the (c) armchair and (d) zigzag directions.

4. Conclusion

We present rigorous assessment on device performances of monolayer black arsenic n- and p-MOSFETs using our *ab-initio*-based *in-house* ballistic transport simulator. Dependency on the transport direction, scaling behavior and the influence of individual Γ and Δ valleys in monolayer black arsenic on current transport are extensively investigated. In the 10 nm gate length scale, seemingly transfer characteristics of monolayer black arsenic n- and p-MOSFETs appear very similar. We observe decent *SS* and maximum and minimum values of I_{ON} in the armchair and zigzag directions, respectively. But, in n- and p- MOSFETs, the main valleys that inject carriers into channel are different. In the case of n-MOSFETs, the highly anisotropic Γ valley corresponding to the valley of CBM is the main valley forming the I_{ON}. Therefore, even if there are isotropic Δ valleys, the dependence of I_{ON} on the direction of transport can be clearly confirmed. In the case of p-MOSFETs, most of the I_{ON} comes from Δ valley, which corresponds to the valley of VBM. However, since both Δ and Γ valleys are anisotropic in VB and the energy separation between Δ and Γ valleys is smaller than in CB, even stronger anisotropy in I_{ON} is obtained. Regarding I_{OFF}, the TN current in I_{OFF} is marginally managed or well suppressed, depending on the transport direction, and hence fairly decent *SS* is achievable. In the 7 nm gate length scale, however, the direct tunneling from source to drain issue in the subthreshold conduction becomes critical. In the case of n-MOSFETs, the TN current from the anisotropic Γ valley in CB is minimized in the zigzag direction. But, the isotropic Δ valleys in CB forms a significant amount of TN current irrespective of channel orientations, consequently deteriorating *SS* equally in all directions. Meanwhile in the case of p-MOSFETs, both Δ and Γ valleys of VB are anisotropic. Therefore, *SS* sharply increases or is still well controlled, depending on the channel orientation. Compared to monolayer black phosphorus, the additional Δ valleys near Γ valley of monolayer black arsenic not only lowers I_{ON} but also makes *SS* worse in the scaled device.

References

[1] Li, L. K.; Yu, Y. J.; Ye, G. J.; Ge, Q. Q.; Ou, X. D.; Wu, H.; Feng, D. L.; Chen, X. H.; Zhang, Y. B. Black Phosphorus Field-Effect Transistors. *Nat. Nanotechnol.* **2014**, 9, 372−377.

[2] Liu, H.; Neal, A. T.; Zhu, Z.; Luo, Z.; Xu, X.; Tománek, D.; Ye, P. D. Phosphorene: An Unexplored 2D Semiconductor with a High Hole Mobility. *ACS Nano* **2014**, 8, 4033–4041.

[3] Qiao, J.; Kong, X.; Hu, Z.-X.; Yang, F.; Ji, W. High-Mobility Transport Anisotropy and Linear Dichroism in Few-Layer Black Phosphorus. *Nat. Commun.* **2014**, 5, 4475

[4] Tao, J.; Shen, W.; Wu, S.; Liu, L.; Feng, Z.; Wang, C.; Hu, C.; Yao, P.; Zhang, H.; Pang, W.; Duan, X.; Liu, J.; Zhou, C.; Zhang, D. Mechanical and Electrical Anisotropy of Few-Layer Black Phosphorus. *ACS Nano* **2015**, 9, 11362−11370.

[5] Lee, S.; Yang, F.; Suh, J.; Yang, S.; Lee, Y.; Li, G.; Choe, H. S.; Suslu, A.; Chen, Y.; Ko, C. Anisotropic in-Plane Thermal Conductivity of Black Phosphorus Nanoribbons at Temperatures Higher Than 100 K. *Nat. Commun.* **2015**, 6, 8573.

[6] Das, S.; Zhang, W.; Demarteau, M.; Hoffmann, A.; Dubey, M.; Roelofs, A. K. Tunable Transport Gap in Phosphorene. *Nano Lett.* **2014**, 14 (10), 5733–5739.

[7] Wood, J. D.; Wells, S. A.; Jariwala, D.; Chen, K.-S.; Cho, E.; Sangwan, V. K.; Liu, X.; Lauhon, L. J.; Marks, T. J.; Hersam, M. C. Effective Passivation of Exfoliated Black Phosphorus Transistors against Ambient Degradation. *Nano Lett.* **2014**, 14, 6964−6970.

[8] Pumera, M.; Sofer, Z. 2D Monoelemental Arsenene, Antimonene, and Bismuthene: Beyond Black Phosphorus. *Adv. Mater.* **2017**, 29, 1605299.

[9] Kamal, C.; Ezawa, M. Arsenene: Two-dimensional Buckled and Puckered Honeycomb Arsenic Systems. *Phys. Rev. B* **2015**, 91, 085423.

[10] Zhang, S.; Xie, M.; Li, F.; Yan, Z.; Li, Y.; Kan, E.; Liu, W.; Chen, Z.; Zeng, H. Semiconducting Group 15 Monolayers: A Broad Range of Band Gaps and High Carrier Mobilities. *Angew. Chem., Int. Ed.* **2016**, 55, 1666−1669.

[11] Zhang, S.; Yan, Z.; Li, Y.; Chen, Z.; Zeng, H. Atomically Thin Arsenene and Antimonene: Semimetal−Semiconductor and Indirect− Direct Band-Gap Transitions. *Angew. Chem., Int. Ed.* **2015**, 54, 3112− 3115

[12] Wang, Y.; Huang, P.; Ye, M.; Quhe, R.; Pan, Y.; Zhang, H.; Zhong, H.; Shi, J.; Lu, J. Many-body Effect, Carrier Mobility, and Device Performance of Hexagonal Arsenene and Antimonene *Chem. Mater.* **2017**, 29, 2191–2201

[13] Pizzi, G.; Gibertini, M.; Dib, E.; Marzari, N.; Iannaccone, G.; Fiori, G. Performance of arsenene and antimonene double-gate MOSFETs from first principles *Nat. Commun.* **2016**, 7, 12585

[14] Sun, X.; Song, Z.; Lu, S.; Wang, Y.; Li, Y.; Wang, W.; Lu, Jing. Sub-5 nm Monolayer Arsenene and Antimonene Transistors *ACS Appl. Mater. Interfaces* **2018**, 10 (26), 22363–22371

[15] Seo, D.; Chang, J. ″Doping-Free Arsenene Heterostructure Metal-Oxide-Semiconductor Field Effect Transistors Enabled by Thickness Modulated Semiconductor to Metal Transition in Arsenene", *Scientific Reports* **2019**, 9 3988

[16] Chen, Y.; Chen, C.; Kealhofer, R.; Liu, H.; Yuan, Z.; Jiang, L.; Suh, J.; Park, J.; Ko, C.; Choe, H.S.; Avila, J.; Zhong, M.; Wei, Z.; Li, S.; Gao, H.; Liu Y.; Analytis, J.; Xia, Q.; Asensio,

M. C.; Wu, J. Black Arsenic: A Layered Semiconductor with Extreme In-Plane Anisotropy *Adv. Mater.* **2018**, 30, 1800754

[17] Zhong, M.; Xia Q.; Pan L.; Liu Y.; Chen, Y.; Deng, H. X.; Li, J.; Wei, Z. Thickness-Dependent Carrier Transport Characteristics of a New 2D Elemental Semiconductor: Black Arsenic *Adv. Funct. Mater.* **2018**, 28, 1802581

[18] Wang, G.; Pandey, R.; Karna, S. P. Atomically thin group V elemental films: Theoretical investigations of antimonene allotropes *ACS Appl. Mater. Interfaces* **2015**, 7, 11490–11496

[19] Kecik, D.; Durgun, E.; Ciraci, S. Stability of Single-layer and Multilayer Arsenene and their Mechanical and Electronic Properties. *Phys. Rev. B: Condens. Matter Mater. Phys.* **2016**, 94, 205409

[20] Xu, Y.; Peng, B.; Zhang, H.; Shao, H; Zhang, R.; Zhu, H. First-principle calculations of optical properties of monolayer arsenene and antimonene allotropes *Ann. Phys.* **2017**, 529, 1600152

[21] Ozaki, T.; Kino, H. Efficient projector expansion for the ab initio LCAO method. *Phys. Rev, B.* **2005,** 72, 045121

[22] Perdew, J. P.; Wang, Y. Accurate and simple analytic representation of the electron-gas correlation energy. *Phy. Rev. B.* **1992**, 45, 13244

[23] Usuki, T.; Saito, M.; Takatsu, M.; Kiehl, R. A.; Yokoyama, N. Numerical analysis of ballistic-electron transport in magnetic fields by using a quantum point contact and a quantum wire. *Phy. Rev. B.* **1995**, 52, 8244-8255

[24] See http://www.itrs.net/ for Process Integration, Devices, and Structures (PIDS), International Technology Roadmap for Semiconductors (ITRS)

[25] Chang, J. Modeling of anisotropic two-dimensional materials monolayer HfS_2 and phosphorene metal-oxide semiconductor field effect transistors *J. Appl. Phys.* **2015**, 117, 214502

[26] Cao, X.; Guo, J. Simulation of Phosphorene Field-Effect Transistor at the Scaling Limit. *IEEE Trans. Electron Devices* **2015**, 62, 659−665